Engineering Structures 228 (2021) 111534

Contents lists available at ScienceDirect

Engineering Structures

journal homepage: www.elsevier.com/locate/engstruct

Rocking of offshore lighthouses under extreme wave impacts: Limit analysis, analytic formulations and distinct element method

Athanasios Pappas [a], Dina D'Ayala [a,*], Darshana T. Dassanayake [b,d], Alessandro Antonini [c], Alison Raby [b]

[a] Civil, Environmental and Geomatic Engineering, University College London, Gower Street, WC1E 6BT London, UK
[b] School of Engineering, Computing and Mathematics, University of Plymouth, Drake Circus, PL4 8AA Plymouth, UK
[c] Faculty of Civil Engineering and Geosciences, Delft University of Technology, Stevinweg 1, 2628 CN Delft, the Netherlands
[d] Department of Civil and Environmental Technology, Faculty of Technology, University of Sri Jayewardenepura, Pitipana, Sri Lanka

ARTICLE INFO

Keywords:
Limit analysis
Distinct element method
Historic lighthouse
Rocking
Wave impact

ABSTRACT

This study describes the structural response of historic lighthouses to extreme wave impacts. Located offshore on exposed rocks, 19th Century lighthouses were built with large interlocked granite blocks and have survived weathering for nearly two centuries. Under extreme wave impacts, lighthouses of this structural typology may uplift and rock, whereas sliding is prevented by the vertical interlocking. The uplift and sliding thresholds calculated with the limit analysis method reveal why this structural system is capable of bearing extreme wave impacts without failure. The ingenious vertical keying is proven to be a major characteristic that contributes to the resilience of these lighthouses. The structural response is explained with the use of analytic formulations of the rocking motion. Detailed analysis of the response to wave impact is conducted with reference to Wolf Rock lighthouse. The impact wave corresponding to a 250-year effective return period is identified using non-stationary Bayesian extreme analysis. Moreover, wave flume tests on a scaled cylindrical structure were performed to identify the wave impact force time-history shapes. Based on two waves: a theoretical time-history based on existing models in the literature and the measured time-histories from small-scale experiments, a series of synthetic force time-history sequences are generated for the purposes of a parametric analysis. This parametric analysis, with the Distinct Element Method, using the commercial software 3DEC, reveals the influence of the duration and shape of the force time-history function. For impacts with the same impulse values, shorter time impacts produce the most intense opening of joints, despite causing smaller horizontal displacements. Furthermore, variability in the structural response is revealed even for impacts of the same impulse, duration and maximum force but different shape of the force time-history.

1. Introduction

In the period between mid-seventeen century to late nineteen century, engineering knowledge of offshore lighthouses evolved, pushed by the need for robust beacons at sea due to the increased maritime traffic associated with the industrial revolution, and the cycles of failures and design improvements that such failure demanded. John Smeaton's design of Eddystone lighthouse, a curved concave profile masonry structure with large-scale interlocked granite blocks which was completed in 1759, was the most significant breakthrough in lighthouse engineering [1]. Eddystone lighthouse survived intact for more than one century on the same rock where three earlier designs had failed, only to be replaced due to a fracture of the foundation rock. Smeaton's main design principles had proved so successful that they were adopted for all heavily exposed lighthouses around the British Isles and Ireland, including Wolf Rock lighthouse which is the object of this study [2]. Victorian engineers were aware that a "*lighthouse-tower might be destroyed in either of two ways, either by being moved bodily by the sliding of the base upon its foundation, or by being fractured at some point in its height, and the upper portion being overthrown*" [3]. The conditions triggering failure by sliding or uplifting, so eloquently identified through empirical observations, can nowadays be quantified by using the concepts of limit analysis, provided sufficient knowledge of the geometry and mass of the structure and also the wave impact force and location, is available.

* Corresponding author.
E-mail address: d.dayala@ucl.ac.uk (D. D'Ayala).

https://doi.org/10.1016/j.engstruct.2020.111534
Received 4 March 2020; Received in revised form 25 July 2020; Accepted 3 November 2020
Available online 7 December 2020

The intensity, force time-history and force distribution of ocean-wave's impact still remain challenges on which much research is devoted. The first major breakthrough in estimation of wave forces on cylindrical structures in the open ocean came approximately 80 years after the inauguration of Wolf Rock lighthouse. Morison et al. (1950) developed a formula to estimate the forces exerted on a circular monopile exposed to deeper water waves. Since then, there have been numerous studies on breaking wave forces on vertical cylinders on horizontal or uniformly sloping seabed. Only a few studies have been conducted to understand the effect of a shoal on breaking wave forces on vertical cylinders ([4–13]). Hall [14] performed the first laboratory experiments aimed to characterize the breaking wave forces on a circular pile located on a sloping beach. Goda [15] investigated breaking wave forces on a vertical cylinder fixed on a reef, however, there are no measurements of impulsive loads. 3D physical modelling studies have been performed to find wave loads on vertical cylinders and concrete tripod structures erected on a submerged shoal/reef ([16,17]). They developed simple formulae to estimate wave forces and moments on a vertical cylinder on a reef, but were limited to the tested conditions of plunging breaking at a submerged reef on a particular geometry and submergence depth.

The original Morison's formula was developed for non-breaking waves, where the total force is a summation of drag force (F_D) and inertia force (F_M). Morison's equation is generally valid for slender cylinders with the ratio of wavelength to member diameter larger than 5. Later, it was revealed that the total force exerted on an offshore monopile can be much higher than that predicted by the Morison's equation. This higher force occurs when a wave breaking onto the cylinder initially exerts a slamming force for a fraction of a second, which is followed by a less impulsive pressure. Therefore, breaking wave forces can be divided into two components, an impact force (or slamming force) component and a quasi-static component. The quasi-static components can be fully described using Morison's equation, but the impact force due to breaking waves can be several times the Morison's forces [18]. Slamming of violently breaking waves onto offshore structures is a strongly nonlinear phenomenon governed by interactions between water, air and the structure. Slamming forces are affected by various factors, such as the compressibility of water, the dynamic of the structure, entrapped air bubbles, cavitation and aeration etc. [19]. Several approaches to estimate the slamming force have been proposed, mostly based on scaled experimental investigations. Slamming force models, developed in [20,21,10], significantly improve the estimation of slamming force on cylindrical structure. However, dedicated experimental or numerical hydrodynamic modelling studies on offshore rock lighthouses were carried out only in [22–24]. Banfi [24] performed experimental investigations using a simplified cylindrical model to study the broken wave impact on Eddystone Lighthouse and its responses to wave loading. It was observed that the incoming waves were breaking away from the lighthouse and only the bore, generated by the breaking waves, was hitting the structure. However, some other rock lighthouses such as Wolf Rock and Bishops Rock are situated on much smaller rock pinnacles and the rock slopes are much steeper. Therefore, Dassanayake et al [25], as part of the STORMLAMP project, performed further experiments in the wave flume of the COAST Laboratory at University of Plymouth with three different foreshore slopes 1:1, 1:2.5 and 1:5. Experimental force time-histories used in the current study were drawn from these small-scale tests.

The lack of knowledge on the wave impact characteristics and the absence of advanced analysis tools have led to the under-design of some offshore lighthouses. Such an example is the Bishop Rock, which was completed in 1858 but soon experienced considerable rocking vibration and fracture of some dioptric apparatus prisms [26]. Between 1883 and 1887 the structure was increased in height and strengthened with an additional external layer of interlocked granite blocks in order to improve resistance to wave impacts. Although the first Bishop Rock lighthouse did not collapse, its improvement in a second stage is a clear example of how lighthouse engineering evolved based on a trial and error empirical approach, as more lighthouses were built during the latter part of the 19th century. It was only one century later that Housner introduced the first analytic formulations for studying the rocking behaviour of slender structures [27]. Housner's work, although focused on ground excitation and not on lateral wave impacts, postulated that the structural behaviour of bodies capable of uplifting differs significantly from the one of continuous structures. Later research confirmed this theory and shed more light on the complexity of the rocking behaviour [28–31]. The rocking theory can explain why lighthouses built with interlocked masonry, presented in this paper, can survive impacts of much higher force levels than what is expected for continuous structures. However, almost all available studies are focused on ground acceleration, thus requiring adaptations in order to analyse the rocking behaviour for lateral loading such as wave impacts. Moreover, the fact that the lighthouses are not monolithic or multi-drum structures with only few blocks, but are instead complex structural systems with a large number of courses and interlocked blocks, makes impractical the precise description of the rocking response using analytical formulations. In order to analyse such complex multi-block structural problems, the Distinct Element Method (DEM) was developed by Cundall [32]. The DEM is an efficient approach to reproduce the structural response of rigid bodies characterised by large displacements and separation between blocks [33,34].

Given the above extensive but rather inconclusive research advances to date, the scope of this study is to shed some light on the implications of selecting a representative wave force time-history profile for studying rocking bodies under lateral impact. The focus is on interlocked masonry lighthouses and the variability of the structural response, which depends on the wave impact characteristics, such as their duration and force time-history shape function. For this purpose, a DEM model of Wolf Rock lighthouse is created and parametric analysis is carried out for different wave impacts. The wave impact profiles are based on wave flume laboratory tests and non-stationary Bayesian extreme analysis on wave data and bathymetry investigations for Wolf Rock reported elsewhere [25,35]. The analytical formulations are used for explaining the structural response caused by the variability of the impact characteristics. Moreover, an application of limit analysis method is proposed as a tool for preliminary assessment of the structural stability in a static approach. It can also provide insight in explaining the importance of the ingenious interlocked masonry lighthouse design which prevents sliding but allows uplift. The methodology adopted and the observations made are presented and discussed in the following sections.

2. Wolf Rock lighthouse and extreme wave impacts

The rock mounted lighthouse of Wolf Rock is located 13 km off the most south-westerly point of Great Britain, between Land's End and the Isles of Scilly. High tides reach up to approximately 4 m from the base of the lighthouse, leaving the structure heavily exposed to ocean waves. Moreover, the steep-sided rock is surrounded by water depths of around 60 m, which means that waves have the potential to reach the tower with little of their energy being dissipated by breaking onto the rocks [35]. The construction of the current lighthouse was initiated in 1862 and completed in 1869. Prior to this structure designed by Douglass, four beacons had been erected and washed aways by violent storms, and a number of other designs for new lighthouses had been abandoned because they could not resist the extreme wave impacts, during construction [2].

Wolf Rock lighthouse has the iconic shape of a concave elliptic frustum, 35.33 m high from foundation to gallery, with a maximum diameter of 12.68 m at its base [2]. The masonry structure consists of six vaulted levels, plus the lantern structure on the top, whereas the lowest 11.98 m are solid except for a water tank (Fig. 1a). A steel frame helideck was mounted on the crown of the masonry structure in the early 1970 s, for facilitating access by lighthouse keepers and later by maintenance

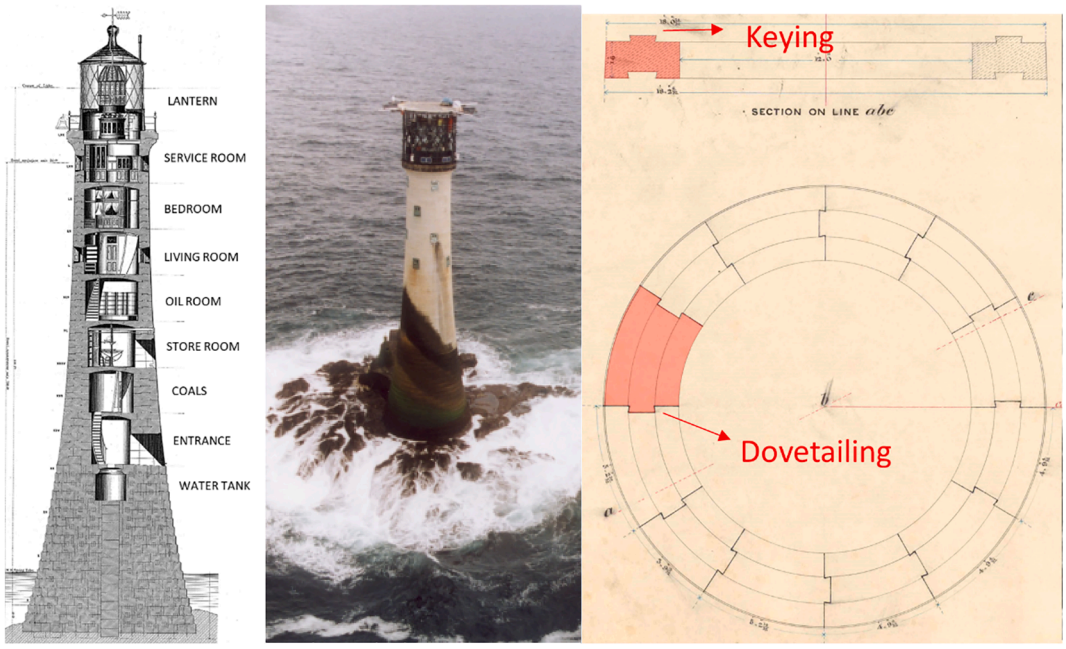

Fig. 1. Wolf Rock lighthouse: (a) original section drawing [2]; (b) contemporary view; (c) details of dovetailing and keying for a course of stones [36].

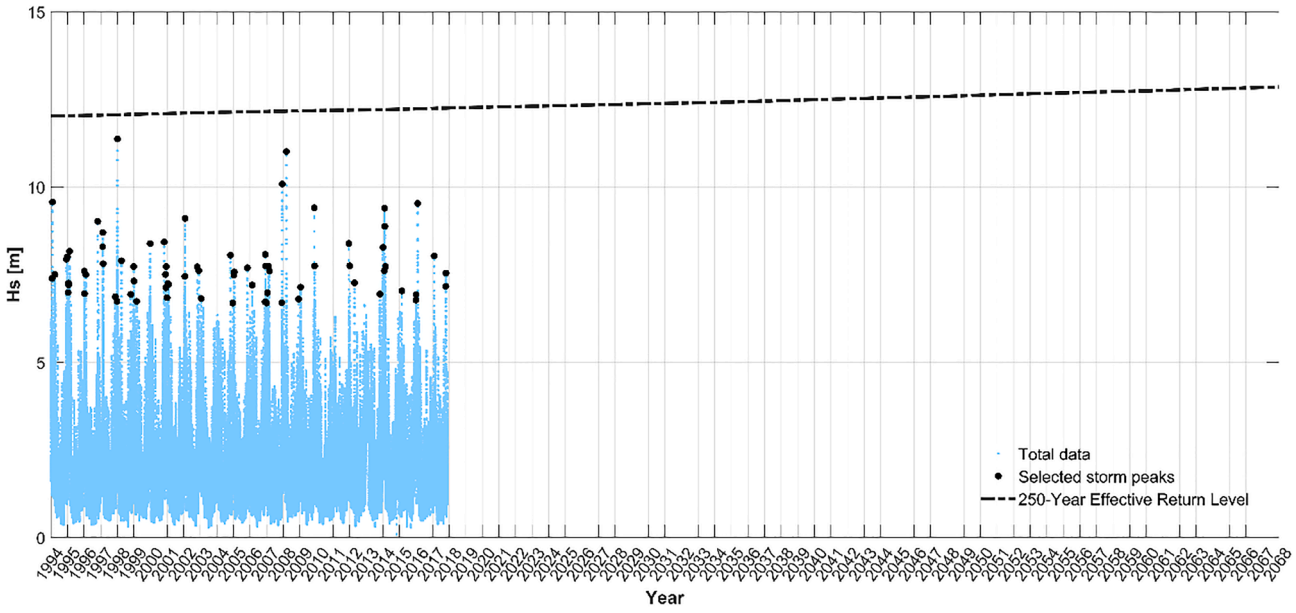

Fig. 2. Wolf Rock Lighthouse effective return levels.

crews when the lighthouses became automated (Fig. 1b). The masonry tower is built with large interlocked granite blocks. The interlocking masonry system, consisting of 12 radially shaped blocks dovetailed in the horizontal plane and tongue and grooved in the vertical plane, is shown in Fig. 1c. Dovetails locks the adjacent wedges of each course whereas vertical keys lock together blocks of consecutive courses. This creates a robust structural system, which is prevented from sliding, but free to uplift, while in each course, it is impossible to remove a block without having removed the adjacent blocks first. The original drawings suggest that the height of the vertical keys is around 76 mm [36].

There are no dedicated empirical or analytical methods to completely describe the breaking or broken wave loadings on exposed cylinder installed on a shoal. The adopted approach for the identification of the design wave height and induced impulsive loading has been

Table 1
250-year effective return period wave height (H_S) projected to 31st December 2067 and induced load (vertical distances measured measured above sea level).

T_R [y]	H_S [m]	T_P [s]	$H_{S.L}$ [m]	D_P [°N]	$H_{0.1\%}$ [m]	η_b [m]	upper loading height [m]	Lower loading height [m]	Load duration [s]	Max force [kN]	Impulse [kN·s]
250	13.85	18.3	13.85	255	25.00	17.99	17.99	9.71	0.068	51,149	1524.91

extensively described in [35,37] and is mainly based on 5 steps that can be summarised as follows:

(i) The design offshore wave climate is described by means of extreme values analysis. The Peak Over Threshold (POT) technique is applied to define the homogenous and independent directional (i.e. same range of directions 195-290° N - dominant direction (D_P) equal to 255° N) extreme events used to fit non-stationary Poisson-Generalised Pareto Distribution (GPD) model, through Bayesian inference. The model is expressed in terms of equivalent Generalised Extreme Value (GEV) distribution, while non-stationarity is introduced to seek to describe the minimal upward trend in extreme wave heights by means of time dependent GEV location parameter through linear trend. The basic idea of the adopted non-stationary approach is to hold the probability of occurrence constant in time, but allowing the return value, i.e. the significant wave heights (H_S), to vary from one time-period to the next. Thus, the concept of effective return level, defined in [38], is used to indicate what significant wave height should be adopted within the considered time interval to have the same risk, Fig. 2.

The dependence between H_S and the peak period (T_P) is described through well-known three-parameter power-law as successfully applied in [39–41]. The final result is a set of *effective return periods* (see Fig. 2), significant wave heights and peak periods describing the offshore wave climate. For the scope of this study, only data corresponding to the 250-year effective wave heights value projected until 2067 are considered (Table 1). All identified values are summarised and described in [34].

(ii) The wave propagation from offshore to the lighthouse location is accounted for by means of the Goda's approach [42], identifying the local significant wave height, ($H_{S,L}$).

(iii) The effects of the depth-induced breaking wave are considered by means of [43], and hence the design breaking wave height is assumed to be $H_{0.1\%}$.

(iv) The crest elevation with respect to the still water level (η_b) is calculated according to Hansen method [44].

(v) Finally, Wienke and Oumeraci method [10] is applied to describe the breaking wave loading time-history, Fig. 3 (referred as "250-year" or "250YR" force time history in this paper).

For a wave impact characterised by 250-year effective return period and projected to the end of 2067, the total impact duration is equal to 0.068 s, and the maximum impact force, at t = 0, is 51,149 kN. The force is applied along a surface comprised between 17.99 m and 9.71 m of heights above the sea level on a frontal section of 60°, with uniform distribution. Thus, the load is applied on 18 courses and the force resultant is applied at a height of 13.85 m above the sea level, or 17.99 above the base of the structure. All details of the considered wave and induced loading conditions are summarised in Table 1.

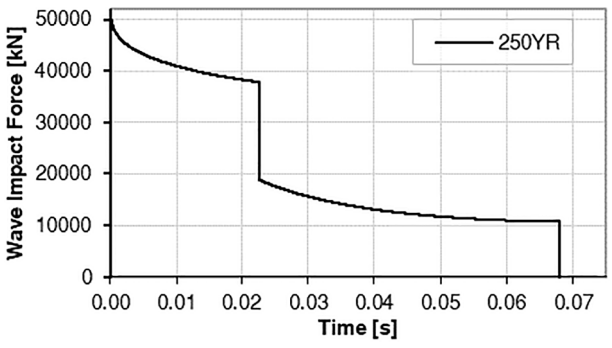

Fig. 3. Time-history of the 250-year effective return values, projected to the end of 2067.

3. Theoretical background

3.1. Limit analysis

The limit state analysis method applied to structures made of rigid blocks [31] allows to calculate the magnitude of a system of forces necessary to trigger a mechanism such as uplift or sliding (Fig. 4a). For uplift, the unbalance of moments around a hinge is calculated between the stabilisation forces, i.e. self-weight, and the external forces. For sliding, the unbalance of forces parallel to a surface is calculated between the stabilisation forces, i.e. friction or bonding forces, and the external forces. When the unbalance is in favour of the external forces, the limit of stability of the structure is reached and the mechanism is triggered. If the forces are not removed failure will ensue due to excessive displacement.

The Principle of Virtual Work (PVW) is a convenient framework to mathematically express such unbalance. Virtual work is the work done by a force acting through a virtual displacement. For the kinematics presented in Fig. 4a, θ and δ are the virtual angle of rotation and virtual horizontal displacement, respectively; whereas F_u and F_s are the activation forces for uplift and sliding, respectively.

According to the PVW, the external virtual work is equal to internal virtual work. Moreover, for rigid bodies, the lack of deformations results in the internal virtual work being equal to zero. Therefore, for the analysed mechanisms of uplift and sliding, Eqs. (1) and (2) are given respectively:

Uplift mechanism:

$$\begin{cases} W_{ext} = F_u h\theta - mgr\theta \\ W_{int} = 0 \end{cases}, \quad W_{ext} = W_{int} \forall \theta \rightarrow F_u = \frac{mgr}{h} \tag{1}$$

Sliding mechanism:

$$\begin{cases} W_{ext} = F_s\delta - F_f\delta \\ W_{int} = 0 \end{cases}, \quad W_{ext} = W_{int} \forall \delta \rightarrow F_s = F_f = \mu \cdot mg \tag{2}$$

where W_{ext} and W_{int} are the work of the external and internal forces respectively; F_f is the friction force; μ is the coefficient of friction; h and r are the vertical and horizontal distance of the centre of mass from the rotational hinge; m and g are the mass of the activated body and the acceleration due to gravity.

Although the equations are simple, the solution is dependent on the location of the hinge or sliding surface, which are not known a-priori, thus making it necessary to analyse all possible positions, i.e. each of the horizontal courses in the masonry that can uplift or slide relative to each other. An iterative algorithm in Python 3.6 programming language is used for calculating the necessary activation force for all possible locations of the hinge and sliding surface at each course along the height of the lighthouse. The condition with the smallest activation force, thus minimum energy, is adopted as the solution to the problem. Solving for all possible wave impact heights and corresponding impact force magnitude, the limit analysis curves of Fig. 4b are obtained. The vertical axis is the height of the resultant wave force and the horizontal axis shows the amplitude of impact force that is necessary for the activation of each failure mechanism. . The activation force required decreases for increasing impact heights, which illustrates the importance of accurately determining the impact height to the structural stability. Wave force-height combinations in the space above these curves signify activation of the respective mechanism.

The force-height combination of the 250-year return period wave calculated for Wolf Rock is represented in Fig. 4b by the diamond dot. For impact resultant at 17.99 m from the base of the structure, the limit state force for uplift is 5734 kN. The wave force of 51,149 kN at 17.99 m exceeds the uplift limit by a factor of approximately 9. Therefore, this wave impact is expected to cause intense uplift and rocking of the Wolf Rock lighthouse. Note that the activation of an uplift mechanism is reversible, meaning that for small duration impacts there can be some

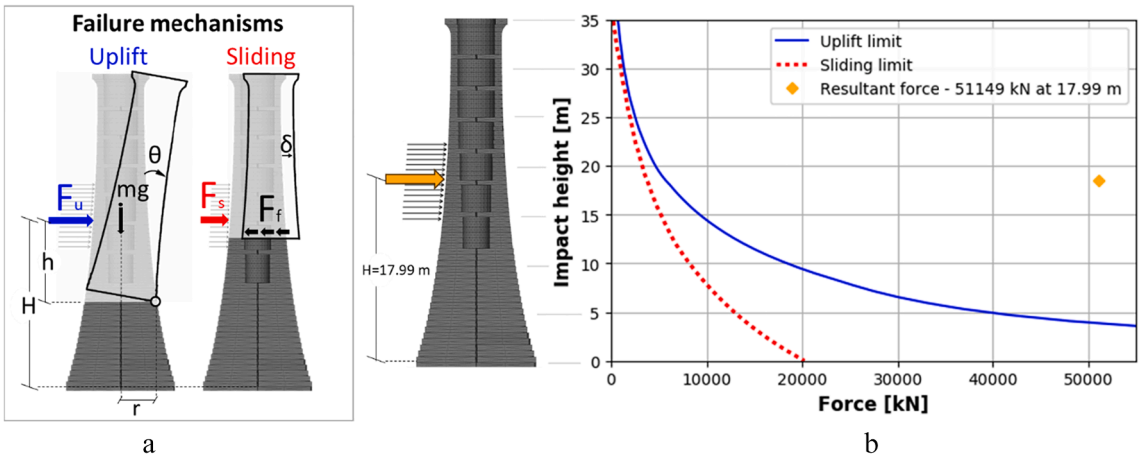

Fig. 4. (a) Failure mechanisms for limit analysis; (b) limit analysis curves and 250-year return period wave impact forces (resultant force-height combination, sliding forces on each course).

uplift and rocking but this does not necessarily result in overturning and collapse [27–29]. The sliding force also exceeds the limit analysis threshold for the sliding mechanisms based on pure friction. However, the vertical interlocking system prevents the sliding which, unlike rocking, is not a self-balancing mechanism and would cause permanent displacement, even though of small magnitude if the impact force is not sustained, and eventually structural failure. Moreover, it is worth noting that the sliding limit is lower than the uplift limit, which suggests that without keying the lighthouse would suffer sliding for impact forces even if they are not sufficient to cause uplift.

A further complication in describing the response of the lighthouse to the wave action, is that, once the initial uplift occurs, depending on the height of impact of the wave and due to the distribution of inertia along the height, other courses can separate from each other and hence the resultant motion is one of multi-body rocking. The set of equations needed to describe this phenomenon are presented in the next section.

3.2. Lighthouse rocking equations for wave impacts

When the lighthouse is impacted by a strong wave able to cause uplift, the structure starts oscillating about a circular hinge created on the opposite side of the impact (Fig. 5a). As a result, the rotating body develops an initial angular acceleration. At the same time, a tangential acceleration a_{tan}, due to the angular acceleration $\ddot{\theta}_{L1}$ acts at any course above O_1. If, for a given distance h_L from O_1, a_{tan} is large enough to cause uplift of the portion of lighthouse above this course, then the system becomes one of two bodies, Lower Body (LB) and Upper Body (UB), rotating with respect to each other (Fig. 5b and 5c). The second circular hinge (O_2) will develop on the opposite side of the first hinge and oscillation of the UB in respect to the LB will be initiated (Fig. 5d). The position of O_2 with respect to the height of lighthouse, is a function of the position of O_1 and the rocking motion determined by the impulse force and its variation in time, therefore it cannot be determined by static equilibrium only.

The equation of rocking motion, developed by Housner [27] for monolithic bodies subjected to ground acceleration, can be applied to the rocking mechanism of a single portion of the lighthouse, as presented in Fig. 5a:

$$I\ddot{\theta}(t) + mg\sqrt{h^2 + r^2}\sin(\alpha - \theta(t)) = F(t)h_F \tag{3}$$

where I is the moment of inertia, h and r are the horizontal and vertical distances of the centre of mass from the hinge of rotation, θ is the rotation angle, $\ddot{\theta}$ is the angular acceleration, α is the critical tilt angle

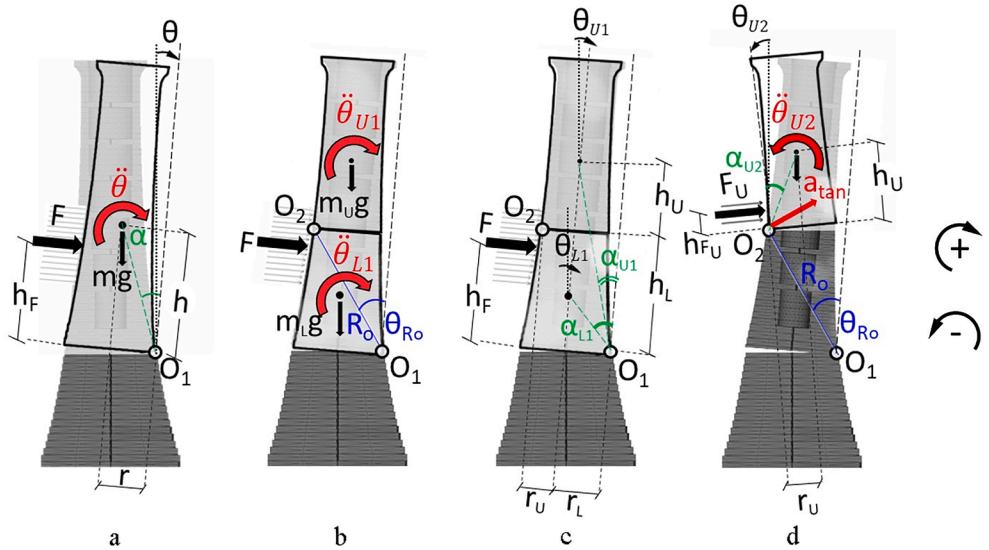

Fig. 5. Rocking of a tapered lighthouse for wave impact: (a) monolithic rocking, (b) rocking of two blocks about the O_1 hinge, (c) geometric properties of rocking bodies, (d) rocking of the UB in respect to the LB about the O_2 hinge.

beyond which equilibrium is lost, F is the resultant of the wave forces, h_F is the distance of F from the hinge, and t is the time.

However, given that joint opening is permitted at all bed joint heights and on both sides of the structure and due to the fact that rocking is a highly dynamic response, a second hinge O_2 may appear on the side opposite to the wave impact, as shown in Fig. 5d. Inertial forces due to the angular acceleration can cause the upper part to rotate about O_1 with a lower angular acceleration ($\ddot{\theta}_{U1}$) than the acceleration of the lower part ($\ddot{\theta}_{L1}$) around the same hinge. This produces a relative rotation of the UB with respect to the LB about O_2.

For the two bodies, i.e. UB and LB, both rotating around O_1 as Fig. 5b, the equation of motion becomes:

$$I_{U1}\ddot{\theta}_{U1}(t) + I_{L1}\ddot{\theta}_{L1}(t) + m_U g\sqrt{(h_U + h_L)^2 + r_U{}^2}\sin(\alpha_{U1} - \theta_{U1}(t)) + m_L g\sqrt{h_L{}^2 + r_L{}^2}\sin(\alpha_{L1} - \theta_{L1}(t)) = F(t)h_F \quad (4)$$

Herein and unless otherwise stated, indexes $_U$ and $_L$ stand for the upper and lower body, respectively. Similarly, indexes $_1$ and $_2$ relate to hinge O_1 and O_2, respectively.

For $\ddot{\theta}_{U1}(t)$ equal to $\ddot{\theta}_{L1}(t)$, which means no relative rotation between the two parts around O_2, and given that $I_{U1} + I_{L1} = I$, Eq. (4) takes the simpler form of Eq. (3).

The rocking motion of the UB can be studied with respect to LB. The rotation of LB creates inertial forces acting on UB. Fig. 5d shows the scheme of this simplified approach with a_{tan} causing the UB to rotate in respect to the LB. The vertical component a_z of a_{tan} offers a stabilising effect for the UB whereas the horizontal component a_x acts as destabilising base acceleration:

$$a_{tan}(t) = \ddot{\theta}_{L1}(t)R_o \quad (5)$$

$$a_x = \ddot{\theta}_{L1}(t)R_o\cos\theta_{R_o} \quad (6)$$

$$a_z = \ddot{\theta}_{L1}(t)R_o\sin\theta_{R_o} \quad (7)$$

where θ_{R_o} is the angle between the vertical and the line from O_1 to O_2 when the bodies are at rest and R_o is the distance between O_1 and O_2. These equations clearly show that the value of the tangential acceleration is a function of R_o and $\ddot{\theta}_{L1}$, and cannot be determined a-priori.

Although this approach cannot be used on its own for fully describing the rocking motion of the structure, due to the fact that there is continuous interaction between the UB and LB that would require defining differential equations for both bodies, it can shed light as to how the response of the UB, and in particular the opening of joints on the opposite side of the wave impact, is influenced by the geometry of the lighthouse and the wave force. With the definitions set in Eqs. (5)–(7), the equation that describes the motion of the UB when rotating about the hinge O_2 of Fig. 5d becomes:

$$I_{U2}\ddot{\theta}_{U2}(t) + m_U(a_z(t) + g)\sqrt{h_U^2 + r_U^2}\sin(-\alpha_{U2} - \theta_{U2}(t)) + F_U(t)h_{FU} = m_U a_x(t)\sqrt{h_U^2 + r_U^2}\cos(-\alpha_{U2} - \theta_{U2}(t)) \quad (8)$$

where F_U is the resultant force of the portion of wave impacting above point O_2 for the body at rest and h_{FU} is the distance of the point of application of the resultant F_U from O_2.

The threshold value of $\ddot{\theta}_{L1}(t)$ that will trigger uplift of the UB with respect to LB is found by setting $\ddot{\theta}_{U2}(t) < 0$ in Eq. (8).

For the impact instant ($t_0 = 0$, $\theta_{U2}(0) = 0$):

$$\sqrt{h_U^2 + r_U^2}\cos(-\alpha_{U2}) = h_U \quad (9)$$

$$\sqrt{h_U^2 + r_U^2}\sin(-\alpha_{U2}) = -r_U \quad (10)$$

With the use of Eqs. (6), (7), (9), (10) and resolving Eq. (8) for $\ddot{\theta}_{U2}(t_0)$, Eq. (8) becomes:

$$\ddot{\theta}_{U2}(t_0) = \frac{1}{I_{0U}}[m_U\ddot{\theta}_L(t_0)R_o(-h_U\cos\theta_{R_o} + r_U\sin\theta_{R_o}) + m_U r_U g + F_U(t_0)h_{FU}] \quad (11)$$

In order to investigate whether $\ddot{\theta}_{L1}(t_0)$ and $\ddot{\theta}_{U2}(t_0)$ are directly or inversely proportional, the following can be assumed: $C_1 = \frac{1}{I_{0U}}m_U R_o$, $C_2 = \frac{1}{I_{0U}}[m_U r_U g + F_U(t_0)h_{FU}]$, where C_1 and C_2 are constants.

Hence, Eq. (11) transforms to:

$$\ddot{\theta}_{U2}(t_0) = \ddot{\theta}_{L1}(t_0)(-h_U\cos\theta_{R_o} + r_U\sin\theta_{R_o})C_1 + C_2 \quad (12)$$

Therefore for $\ddot{\theta}_{L1}(t_0)$ to have a destabilising effect on UB, inverse proportionality between $\ddot{\theta}_{L1}(t_0)$ and $\ddot{\theta}_{U2}(t_0)$ is needed. Therefore, from Eq. (12) the condition for inverse proportionality becomes:

$(-h_U\cos\theta_{R_o} + r_U\sin\theta_{R_o})C_1 < 0$

Because C_1 is a positive constant, it follows that:

$$-h_U\cos\theta_{R_o} + r_U\sin\theta_{R_o} < 0$$

which leads to:

$$\frac{\sin\theta_{R_o}}{\cos\theta_{R_o}} < \frac{h_U}{r_U} \quad (13)$$

From the geometry of the UB shown in Fig. 5d, Eq. (13) gives:

$$\theta_{Ro} < \frac{\pi}{2} - \alpha_{U2} \quad (14)$$

Therefore, Eq. (14) demonstrates that if θ_{Ro} is smaller than $\frac{\pi}{2} - \alpha_{U2}$, then $\ddot{\theta}_{L1}(t_0)$ has a negative effect to the stability of the UB, i.e. it triggers counter clockwise rotation of the UB and opening of a second joint on the opposite side of the wave impact. Eq. (14) provides a geometric condition for the relative size of the two portions of the lighthouse body, rocking on each other.

As already mentioned, given the nonlinearity in the shape of the lighthouse, the dependence of the formation of successive hinges on the location of the first hinge, itself a function of location, magnitude and duration of the wave impact's resultant force, and the dynamic nature of each of these variables, the above equations cannot be easily solved. Therefore, a discrete element model is proposed to further analyse the response of the lighthouse to wave impact.

4. Parametric analysis on force time-history functions with DEM

Given the large number of unknowns identified for both the forcing wave and the response of the lighthouse, and given that each of the parameters describing such interaction is affected by both epistemological and aleatoric uncertainties, the study is pursued by performing a parametric analysis of time histories of the lighthouse modelled using the Discrete Element Method approach. In the following the specific strategy adopted for the numerical modelling are first described, these parameters being taken as constant and nominal value resulting from previous studies as indicated in section 4.1. As the variability in the wave impact is the aspect most affected by uncertainty, the analysis conducted herein considers the effect of impulse magnitude and duration and wave shape as the parameters affecting the response. For the results of these analyses to be comparable an efficient measure, the *angular impulse*, is proposed which represent fully the intensity of the impacting wave. Results are discussed in terms of maximum lateral displacement and uplift.

4.1. DEM model description

The three-dimensional numerical model of the lighthouse is developed with the use of the Distinct Element Method (DEM) software 3DEC

which adopts an explicit numerical solution [45]. To reproduce the real configuration, the structure is modelled with a uniform number of 12 blocks per course (Fig. 6). Each vertical joint coincides with the mid-edge of the blocks below and above it, forming continuous blockwork able to reproduce the structural behaviour of the real lighthouse. The vertical keys, of height equal to 76 mm, are also modelled in detail. The dovetailing between blocks of the same course is not modelled, to expedite the construction of the model and to reduce runtime, by reducing the number of contact surfaces, however, the presence of the vertical keys guarantees the structural integrity and, given the circular shape, it is sufficient to prevent relative dislocation between blocks unless a very intense uplift, i.e. greater than the key height, takes place. A tight fit (zero gap) is assumed for the keys and grooves, which creates a modest resistance to uplift, thus indirectly modelling the effect of cohesion due to the mortar in the groove.

Although all blocks are rigid, the structure's elastic characteristics are accounted for by defining a finite stiffness for the contact interfaces. The normal stiffness of the horizontal joints is calibrated based on the results of field modal tests [46,47]. The spring of the horizontal joints are given normal stiffness equal to $7.31 \cdot 10^{10}$ Pa/m. Accounted for as 69 in-row spring elements, this stiffness value provides an equivalent compressive modulus of elasticity equal to 37 GPa. Zero tensile strength is assumed for the horizontal mortar joints; hence the normal stiffness acts only in compression. Past studies using DEM modelling for analysis of rocking bodies suggest ratios of shear stiffness (k_s) to normal stiffness (k_n) between 0.5 and 1.0 [48–51]. Therefore, an intermediate value of $k_s = 0.75k_n$ is taken, resulting to k_s equal to $5.48 \cdot 10^{10}$ Pa/m. The Coulomb friction law, active on all contact surfaces, is implemented with zero cohesion and friction angle of 30°, corresponding to granite - granite contact under high compression levels [52]. The specific weight of the masonry blocks is taken equal to 2463 kg/m^3, which corresponds to granite similar to the one used for the same typology lighthouse of Fastnet Rock [53]. Mass-only Rayleigh damping was applied to match with the field modal tests which provided a damping ratio around 0.75% at 4.67 Hz, the fundamental frequency of the lighthouse.

4.2. Angular impulse for rocking body

In order to study the structural response of the lighthouse to lateral impacts, various wave impact profiles are used. The parametric analysis includes the following wave profiles: the wave obtained from flume laboratory tests; the 250-year return period theoretical wave, introduce in section 2; and a number of synthetic profiles derived from those. To obtain comparable results, the wave profiles are selected and scaled to have equal angular impulse (J_{ang}). The three variables that influence the rocking behaviour of a body under lateral impact are the force, height of application and time period of the impact, hence making J_{ang} an efficient parameter to compare the hazards. For a rotating body, J_{ang} is defined as:

$$J_{ang} = \int_{t_0}^{t_0+\Delta T} (F(t)h - mgr)dt \quad (15)$$

The terms included in the parenthesis of the Eq. (15) also form the Eq. (1) which is used for calculating the uplift threshold for a specific height of impact. This establishes the connection between the uplift mechanism calculated with the linear analysis in section 3.1 and the DEM dynamic analyses presented herein. For the purpose of this study it is assumed that the height of application on the wave resultant is the same for all waves analysed, notwithstanding the uncertainty associated with it, therefore the only element of variability in Eq. (15) is F(t). For a lighthouse in equilibrium, the wave force becomes critical only when it can trigger uplift. Below this threshold, the forces do not contribute to rocking, as will be further discussed in the following.

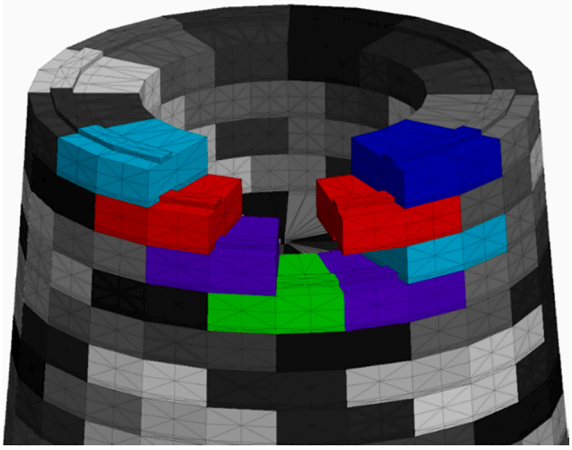

Fig. 6. Interlocked rigid blocks in DEM model.

4.3. Wave flume laboratory testing

Force-time histories used for the current study were acquired during the STORMLAMP project small-scale experiments. The experiments were performed in a wave flume (35 m long × 0.6 m wide × 1.2 m high) in the COAST Laboratory at the University of Plymouth. [25] Fig. 7 illustrates the model setup, which corresponds to 1:81 Froude scale. The size of the model was constrained by the desire to minimize blockage effects in the flume. The shoal geometry was simplified with a 1:5 foreshore slope, a horizontal berm and a 1:1 leeward slope in the physical model. The lighthouse was modelled as a vertical cylinder located at the centre of the horizontal berm and connected to a six-axis load cell. This setup enabled force measurements along three perpendicular axes, with three simultaneous torque measurements about those axes. The Y-axis was aligned with the incoming wave direction, the X-axis was perpendicular to the flume's side walls and the Z-axis was perpendicular to the flume bed. The still water level was coincident with the top of the shoal, i.e. 0.5 m above the flume bed. Water surface elevations offshore of the shoal were recorded using an array of 4 wave gauges (numbers 1–4), which were then used for wave reflection analysis to identify effective incident waves. A further 8 wave gauges measured water surface elevations on the shoal, both on the offshore and leeward side of the model. The model was tested with a range of wave parameters that were selected following analysis of probable extreme wave conditions occurring in the vicinity of Wolf Rock lighthouse [35] and briefly described in section 2. Irregular, regular and focused wave conditions were simulated according to the identified risk level proposed in [35]. Focused waves were based on the New Wave theory [54]. The measured wave force due to the 250 years return period focused wave group, in which the maximum individual wave height was assumed equal to $H_{0.1\%}$ of the underlying Jonswap energy spectrum [43], was scaled up according to the adopted Froude scale, i.e. 1:81, in order to make it commensurable to the theoretical force time-history introduced in section 2.

4.4. Wave profiles

The initial input for the generation of the wave profile are the theoretical force time-history for the 250-year wave, (called 250YR, Fig. 8a) introduced in section 2, and the experimental wave obtained from the flume testing (Fig. 8b), described above. The experimental force time-history was further scaled-up with a factor of 1.19, so as to obtain the same J_{ang} as for the theoretical force time-history. To examine the effect of the time-history function shape and duration on the structural response of the lighthouse, the experimental force time-history (referred as force time history "LAB" in this study) is further manipulated. In detail, while the total impulse and the frequency components of

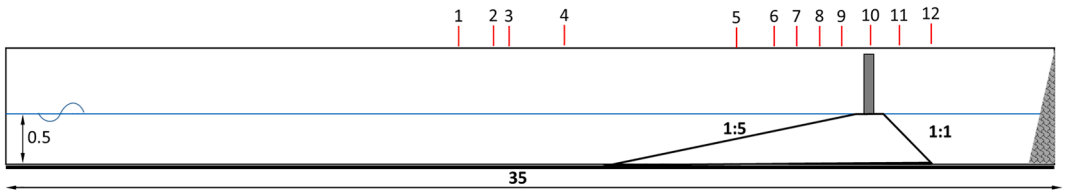

Fig. 7. Experiment setup with wave gauges locations (dimensions are in *m*).

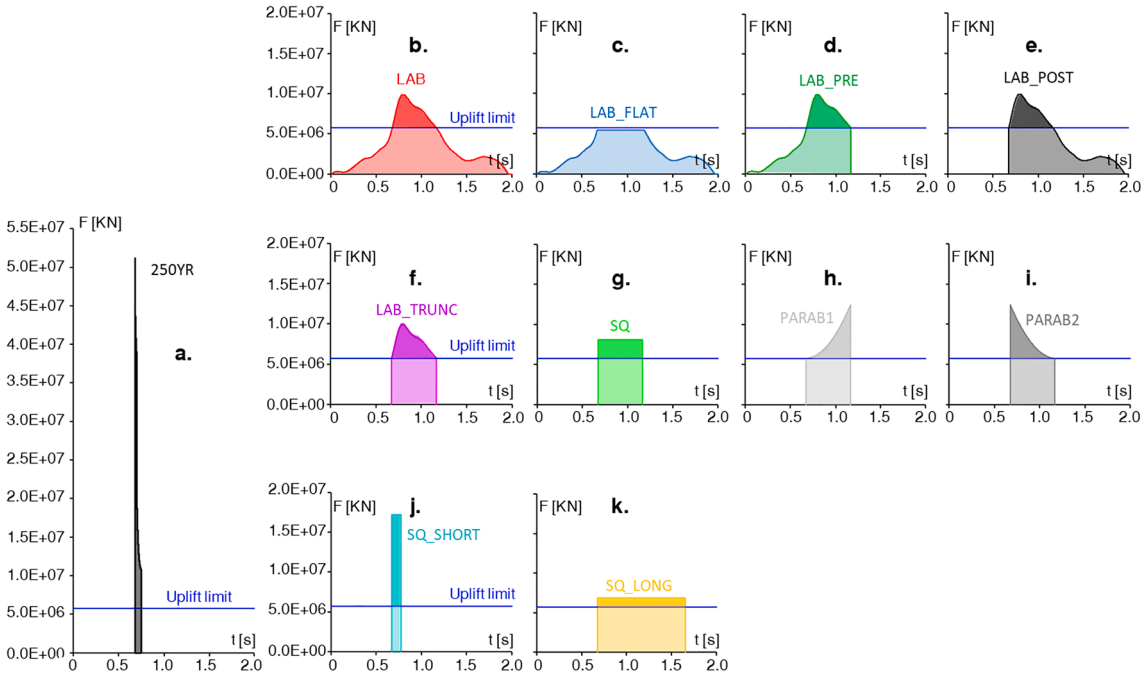

Fig. 8. Force time-history functions for parametric analysis: (a) 250-year return period theoretical impulse wave; (b) scaled from laboratory flume test (c) capped; (d) without the tail; (e) without the initial ramp; (f) truncated; (g) rectangular; (h) parabolic increasing; (i) parabolic decreasing; (j) short rectangular; (k) long rectangular.

the experimental wave signal are preserved, the total duration, the total force above the uplift threshold and consequently the peak force are altered.

As a results, all waves time-histories represented in Fig. 8 have the same J_{ang} with the exception of LAB_FLAT for which the forces are capped at 5447 kN, or 5% lower than the uplift threshold (Fig. 8c). LAB_PRE and LAB_POST (Fig. 8d, 8e) are identical to LAB but without the tail and initial ramp, respectively, thus aiming to study how these affect the structural response. LAB_TRUNC, SQ, PARAB1 and PARAB2 have different magnitude profile, but same overall duration, set equal to 0.491 s, which is the period of time included between the instant at which the LAB time-history first exceeds the uplift threshold at 0.674 s, and the instant at which it drops again under it at 1.164 s. This group of impacts intends to shed some light on the effect of the shape of the time-history function for impacts of the same duration. The effect of the duration is also studied with SQ_LONG and SQ_SHORT time-histories. SQ_LONG time-history has double the duration of the previous group of impacts, i.e. 0.982 s, and SQ_SHORT has a considerably smaller duration equal to 0.1 s (Fig. 8j, 8k), still maintaining the same overall J_{ang}. More details about the wave characteristic and the main structural responses that they yield are presented in Table 2 and further discussed in the following sections.

4.5. Influence of force time-history shape

For the parametric analysis, the results are compared in terms of

Table 2
Wave impact characteristics and response results.

	250YR	LAB	LAB_FLAT	LAB_PRE	LAB_POST	LAB_TRUNC	SQ	PARAB1	PARAB2	SQ_SHORT	SQ_LONG
Total duration [s]	0.068	2.0	2.0	1.164	1.287	0.491	0.491	0.491	0.491	0.1	0.982
Duration of forces over the uplift limit [s]	0.068	0.491	–	0.491	0.491	0.491	0.491	0.491	0.491	0.1	0.982
Peak Force [kN]	51,149	9897	5447	9897	9897	9897	8055	12,450	12,450	17,169	6893
Horizontal displacement on the top [mm]	276.4	574.7	52.3	526.5	591.3	534.9	466.7	429.1	561.1	282.0	537.8
Opening of lower joints on impact side [mm]	15.9	14.0	2.6	14.9	20.4	16.6	15.4	22.5	16.3	17.1	14.0
Opening of upper joints on opposite side to impact [mm]	22.3	0.5	≈0.0	0.4	0.6	0.6	4.3	0.6	4.6	13.8	0.4

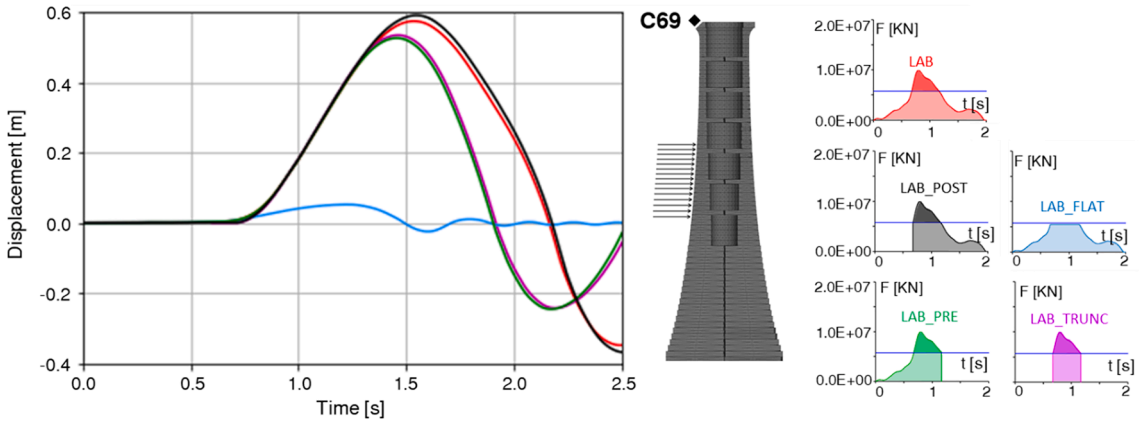

Fig. 9. Horizontal displacement on the top course for LAB, LAB_POST, LAB_PRE, LAB_FLAT, LAB_TRUNC.

horizontal displacements and joint uplift. Fig. 9 presents the horizontal displacement of the top course of the masonry tower for LAB, LAB_POST, LAB_PRE, LAB_FLAT and LAB_TRUNC. These waves are created based on the LAB wave but have parts of the time-history removed. Fig. 9 shows that the response for the LAB_FLAT wave loading remains quite small compared to the other waves. The limit analysis method assumes that the structure is infinitely rigid and therefore no displacement is expected until the exceedance of the force threshold of 5734 kN, irrespective of the length of time the force is applied for. However, the lighthouse and, therefore, the DEM model are not infinitely rigid [55]. As a consequence, for the LAB_FLAT wave the analysis yields horizontal displacement of the top course of the lighthouse equal to 52.3 mm, around 11 times smaller than the maximum horizontal displacement caused by the LAB wave. The value obtained is very close to the static horizontal deflection of a cantilever of equivalent stiffness under the same loading condition. This confirms that the uplift limit is a useful indicator of the structural response.

Fig. 9 shows similarity between the responses obtained for LAB and LAB_POST (red and black) and also between the LAB_PRE and LAB_TRUNC (green and magenta). The first observation, which confirms what observed for LAB_FLAT, is that the ramp from 0.0 s to the uplift threshold, reached at 0.674 s, has minimal effect on oscillation amplitude and period. Conversely, the results show that the tail of the force time-histories, i.e. after 1.164 s when the force drops again below the uplift limit, influences the peak displacement and the period of the oscillation. Impacts without the tail force (LAB_PRE and LAB_TRUNC) produce lower maximum displacements over a shorter oscillation period, compared to the ones caused by the impacts with tail forces (LAB and LAB_POST). To explain this, it is worth remembering that the uplift threshold identifies the time in the loading history when the wave impulse and moment generated by it becomes greater than the stabilising effect of the gravitational forces and the rocking mechanism is triggered. Once the motion is initiated the system becomes dynamic. Therefore, the wave forces of LAB and LAB_POST keep transferring energy to the system, (as seen by the equation of motion Eq. (4) beyond the time 1.164 s, when the resultant moment becomes again smaller than the uplift threshold). In contrast, for LAB_PRE and LAB_TRUNC the wave forces cease after 1.164 s, hence beyond this time only the stabilising gravitational forces are acting on the lighthouse, bringing it back to rest in a time period 0.3 s shorter than seen for LAB and LAB_POST.

The influence of peak force, time history function shape and duration, on the structural response of the lighthouse in shown in Fig. 10 for LAB_TRUNC, SQ, PARAB1, PARAB2, SQ_SHORT and SQ_LONG. The 250YR theoretical wave shape, which has the highest magnitude and shortest impact time, causes the smallest maximum horizontal displacement of the top course, followed by SQ_SHORT that is the second highest magnitude and shortest impact time. In contrast, the SQ_LONG impact, with lowest magnitude and the longest impact time, yields one of the largest displacements of the top course, although with some significant delay with respect to the other wave's shapes. These results indicate the important influence of the impulse duration besides the maximum instantaneous force exerted, in agreement with the substantial inertia of the lighthouse.

In order to explain the influence of the shape and duration of the wave force time-history function it is worth examining the analytic equations. Integrating the Eq. (3) and setting $\sqrt{h^2+r^2}sin(\alpha-\theta(t)) = r$, which is an acceptable simplification for small angles $\theta(t)$, gives:

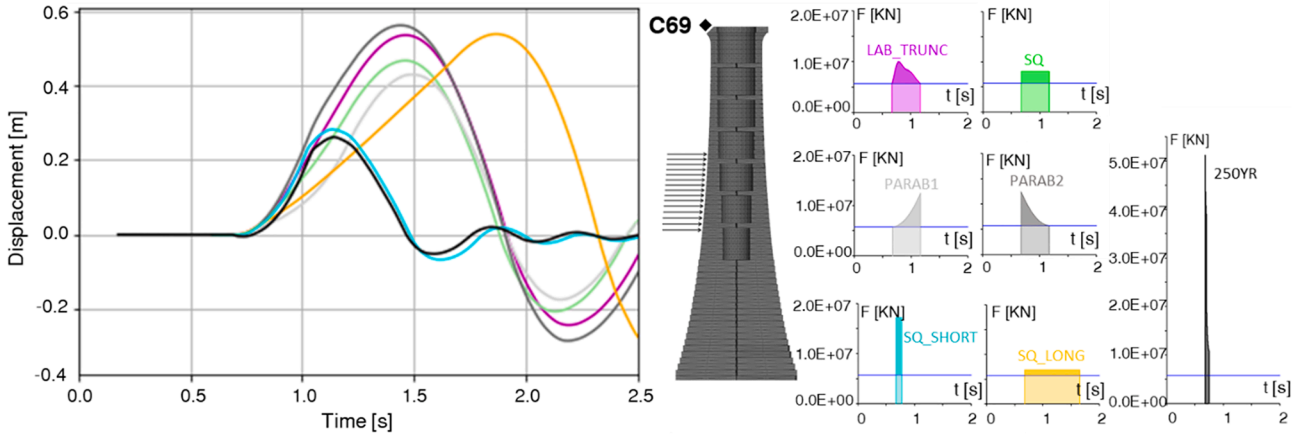

Fig. 10. Horizontal displacement on the top course for LAB_TRUNC, SQ, PARAB1, PARAB2, SQ_SHORT, SQ_LONG.

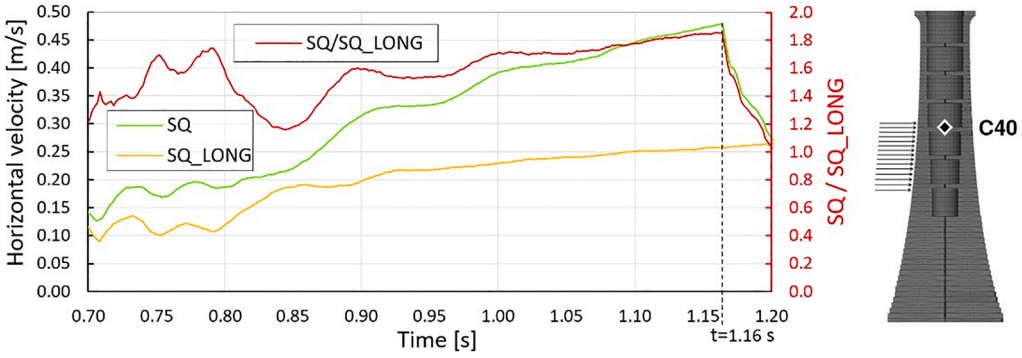

Fig. 11. Response velocities and their ratio for SQ and SQLONG impacts, measured at a control point on the 40th course.

$$\dot{\theta}_i = \frac{h_F \int F_i(t)dt - m \cdot g \cdot r \cdot \Delta t_i}{I} \tag{16}$$

The rotation θ_i is obtained by integrating the $\dot{\theta}_i$ in Eq. (16):

$$\theta_i = \frac{h_F \iint F_i(t)dtdt - m_i \cdot g \cdot r_i \cdot \Delta t_i^2}{2I} \tag{17}$$

From Eq. (16), the ratio of angular velocities $\dot{\theta}_{1w}$ and $\dot{\theta}_{2w}$ caused by two different impulse waves becomes:

$$\frac{\dot{\theta}_{1w}}{\dot{\theta}_{2w}} = \frac{h_F \int_{t0}^{t1} F_1(t)dt - m \cdot g \cdot r \cdot \Delta t_1}{h_F \int_{t0}^{t2} F_2(t)dt - m \cdot g \cdot r \cdot \Delta t_2} \cdot \frac{I}{I} = \frac{J_{ang,1}}{J_{ang,2}} \tag{18}$$

where it is assumed that the geometry of the rocking bodies are the same for the two waves, and $J_{ang,1}$ and $J_{ang,2}$ are the angular impulses.

Comparing the angular velocities caused by SQ_LONG and SQ for equal intervals of time $\Delta t_1 = \Delta t_2$, and before the end of the SQ impact (i.e. t_i between 0.674 s and 1.164 s), and assuming the same rocking parameters for both impacts, as $mgr \cong 0$, then eq. 18 becomes:

$$\frac{\dot{\theta}_{SQ}}{\dot{\theta}_{SQ\_LONG}} = \frac{(h_F \cdot F_{SQ} - m \cdot g \cdot r)\Delta t}{(h_F \cdot F_{SQ\_LONG} - m \cdot g \cdot r)\Delta t} \cong 2 \tag{19}$$

indicating that the initial ratio of the angular velocities achieved under the two impulses is equal to the ratio of the magnitude of the applied forces.

The findings of the DEM analyses show that the relationship between the two velocities is much more complex, and variable with time, when the multi-body interlocked masonry model representing the lighthouse, with changes in position of the hinges, is considered. Fig. 11 shows the variation of the ratio of velocities *SQ*/*SQ_LONG* over time for a control point on the 40th course. The *SQ*/*SQ_LONG* ratio ranges between 1.17 and 1.86. The fact that the ratio is not constant means that there are additional mechanisms that dissipate energy in different amounts for the two impulses.

According to Eq. (16), for impacts such as SQ_LONG and SQ which have constant force, the velocity should be a linear function of time. The graphs of the recorded velocities in Fig. 11 show changes in the gradient of the velocities. For both impulses the velocity tends to increase with time, however the gradient of the curve shows clear fluctuations. These fluctuations are concentrated in the initial part of the event, however for SQ are visible also after 0.9 s. They are less evident for SQ_LONG beyond this point.

The graphs of vertical displacements at each course, shown in Fig. 12, explain the change in velocity gradients. For both responses, the changes in velocity gradient coincide with activity on the lower courses of the lighthouse. With the progression of the rocking response, the rocking motion is slowly propagated to the lower courses of the structure which start uplifting. The activation of these courses increases the I, m,r and h_F of the system, thus requiring a greater impulse to sustain the acceleration of the rocking motion and a constantly increasing speed. In addition, energy is dissipated due to impact between the horizontal courses and friction at the vertical interfaces of the blocks and of the vertical keys.

Another factor that affects the structural behaviour, making the numerical analysis results deviate from the theoretical ratio of the Eq. (19), is the formation of a two-hinge mechanism like the one shown in

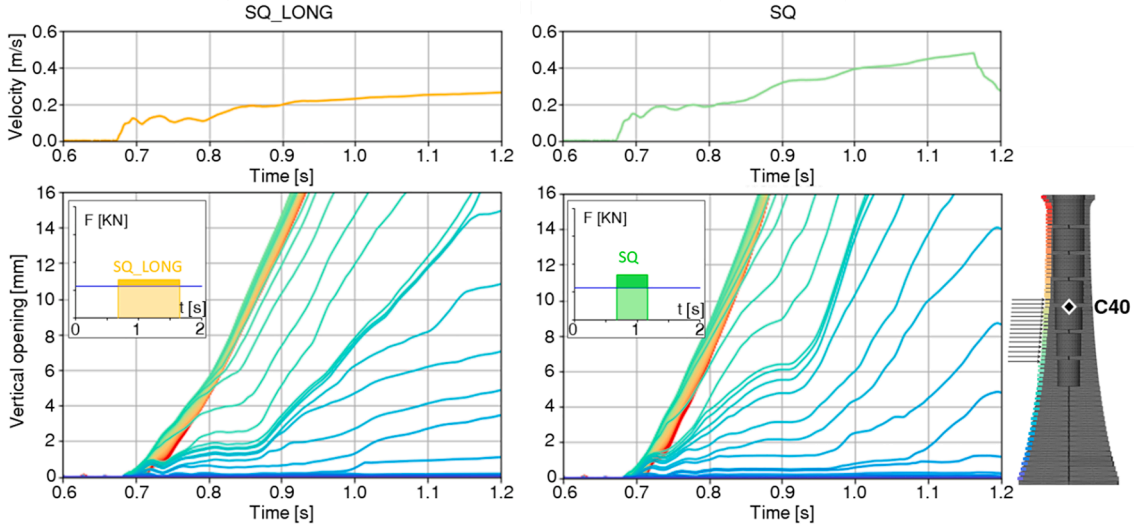

Fig. 12. Responses for the SQ_LONG and SQ impacts: (up) horizontal velocity on the higher vaulted floor; (down) vertical displacements on each course.

Fig. 5d. The opening of joints on the side opposite to the impact takes place for both SQ_LONG and SQ, but it is rather limited. For impulses with higher initial force that cause greater joint uplifts on the opposite side, the deviation from the theoretical ratio becomes greater.

In order to study the effect of the shape of the wave time-histories, the results of waves with the same duration are compared. Fig. 10 shows that impulse with the same duration (LAB_TRUNC, SQ, PARAB1, PARAB2) produce a very different structural response. With PARAB1 and PARAB2 having identical but mirrored shapes this discrepancy is particularly striking. The explanation to this response lays in the opening of joints on the opposite side of the wave impact and the formation of a two-body kinematic mechanism. As shown by Eqs. (13) and (14), for the upper joints of the lighthouse where θ_{Ro} is smaller than $\frac{\pi}{2} - \alpha_{U2}$, the greater the initial angular acceleration $\ddot{\theta}_L$ of the lower part, the more the joints on the opposite side of the wave impact tend to open. Therefore, high initial wave forces cause high initial $\ddot{\theta}_L$ and subsequently more intense rocking of the upper block which leads to higher overall rotations and displacements at the top course.

Fig. 13 shows that for the initial instants of the impulse, roughly between 0.674 s and 0.8 s, PARAB1 yields negligible opening of the upper joints whereas PARAB2 manifests greater openings (maximum equal to 4.3 mm) and rocking of the upper part separately from the lower part. This reveals that the structure impacted by the PARAB1 wave exhibits rocking motion closer to one shown in Fig. 5a whereas for PARAB2 the lighthouse forms a mechanism similar to Fig. 5d, though in both cases the uplift occurs between multiple courses. Towards the end of the impulse duration of the PARAB1 wave though, when the wave force increases, the structure exhibits some new uplift between the upper courses which are slightly higher than the ones recorded at the beginning of the motion. However, these uplifts are still much smaller than the ones caused by the PARAB2 impulse shape. Regarding the courses on the offshore side, the uplift during the early stages of the motion is concentrated on the lower courses (Fig. 14a) for both impulse shapes, however the total uplift is greater for PARAB2 (Fig. 14b) with a higher initial force. Nonetheless the highest single uplift, equal to 22.5 mm occurring at 1.6 s, is caused by PARAB1 slightly after the maximum top horizontal displacement has been achieved and the upper part begins rotating back to the initial position (Fig. 14a).

The same explanation can be used for interpreting the results of Fig. 9, which shows that impulses without a gradual force ramp (i.e. zero force between 0 s and 0.674 s) yield slightly higher lateral displacements than the respective impulse that do not have a sudden increase in force. LAB_POST yields slightly higher displacement than LAB, whereas LAB_TRUNC excites the structure more than LAB_PRE. In order to explain this counterintuitive result, it is worth studying the uplift on the courses on the leeward side. Fig. 15b shows that at the beginning of the motion, LAB_POST causes uplift of courses on the upper portion, between 0.674 s and 0.9 s. For the LAB wave loading, the opening of the same courses remains much smaller (Fig. 15a). As a consequence, for LAB_POST the upper portion manifests a slightly more intense rocking motion in respect to the lower part compared to the LAB, which prompts overall increased lateral displacements of the top courses.

The complex structural response of the lighthouse is more evident when the results of the short duration-high intensity 250YR wave impulse are considered. The DEM analysis shows that, compared to all other waves (with the obvious exception of the capped LAB_FLAT), 250YR yields the lowest level of horizontal displacements of the top courses (Fig. 10). Eq. (17) demonstrates the importance of the impact duration on the structural response. Although 250YR has much higher peak wave force than the other impacts, it has considerably shorter duration and this results in lower overall displacements. However, for this structural typology of lighthouses, it would be a mistake to assume

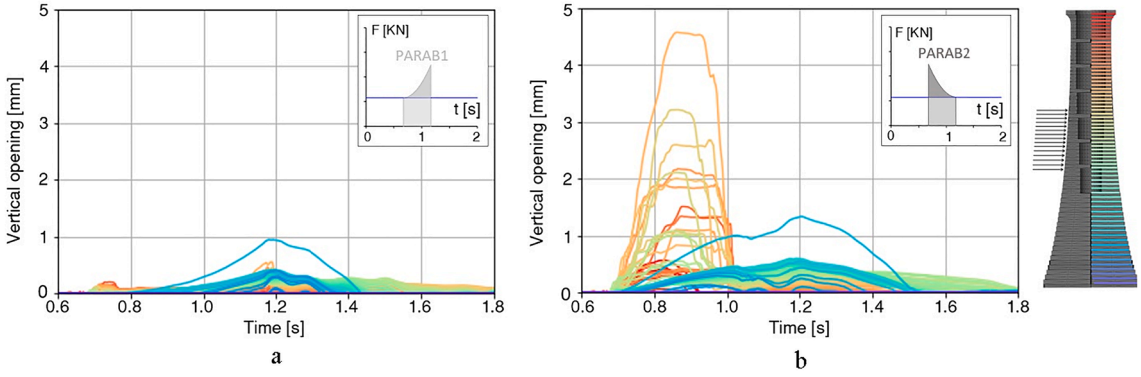

Fig. 13. Individual courses uplift on the leeward side of the incoming wave during the first half-cycle of rocking for: (a) PARAB1; (b) PARAB2. Colour coding refers to the height of the course above sea level as per lighthouse elevation.

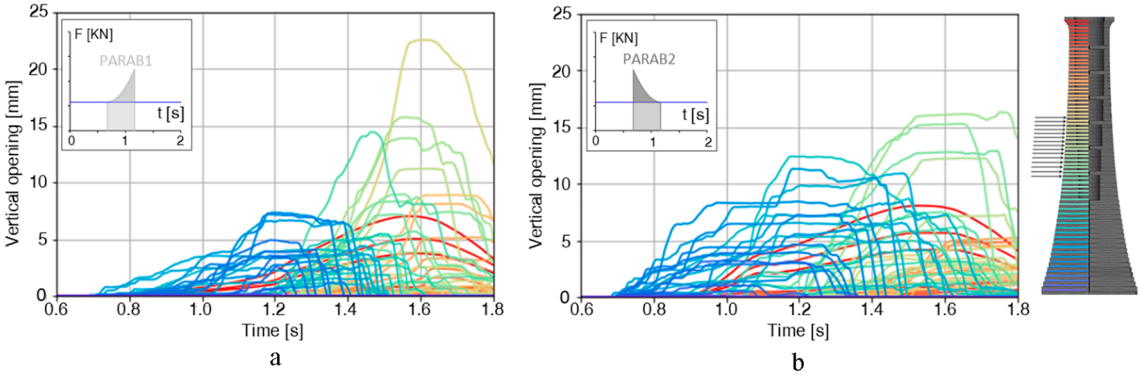

Fig. 14. Individual courses uplift on the offshore side during the first half-cycle of rocking for: (a) PARAB1; (b) PARAB2. Colour coding refers to the height of the course above sea level as per lighthouse elevation.

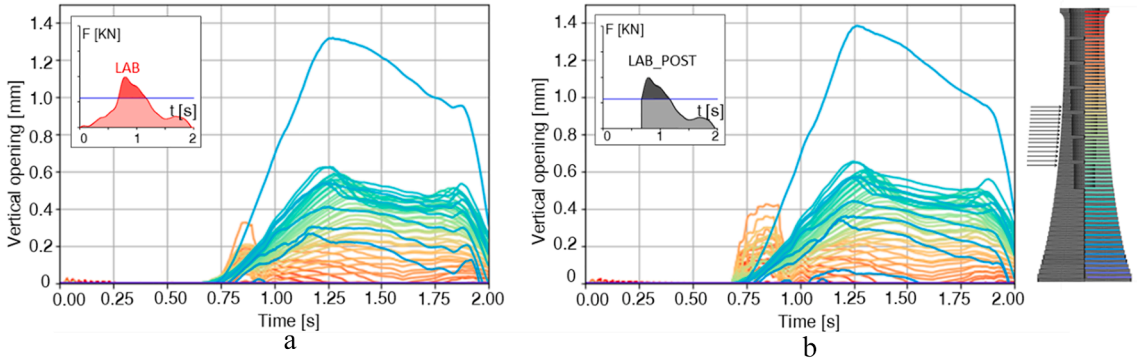

Fig. 15. Individual courses uplift on the leeward side for: (a) LAB; (b) LAB_POST.

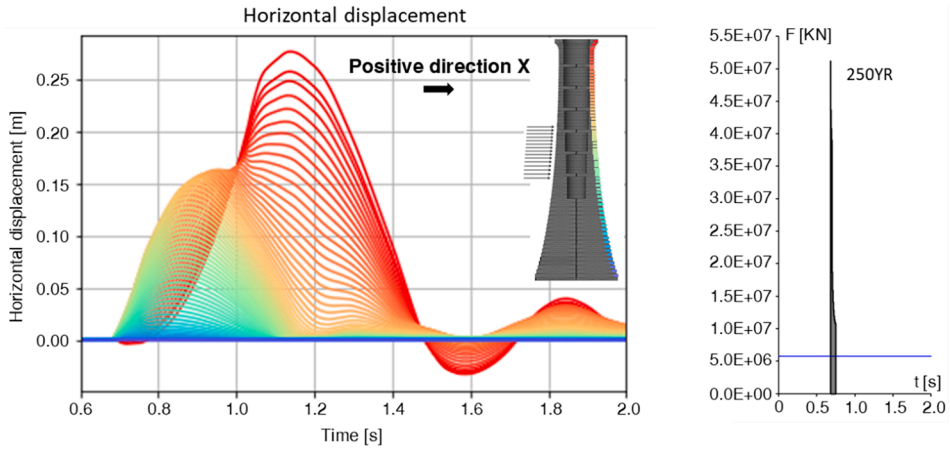

Fig. 16. Horizontal displacements on each course level on leeward side for the 250YR wave.

that because of the lower lateral displacements when compared with other impulse shape, this is a less dangerous wave effect. It was shown earlier that high initial wave forces, such as for 250YR, cause opening of the upper courses on the leeward side and intense rocking of the upper section in respect to the lower section. 250YR causes the leeward side's highest uplift, at 22.3 mm (Table 1). However, this uplift is still considerably lower than the height of the vertical keys that prevents sliding. The limit analysis curve for sliding, shown in Fig. 4b, demonstrates that without the vertical keys the lighthouse would not be able to survive the sliding forces of the 250YR impact.

The tracing of the horizontal displacements in Fig. 16 shows that the lower courses are activated approximately between 0.7 s and 1.2 s. A clear peak lag is evident for the upper courses which show first rocking half-cycle on increasing duration up to 1.5 s, before bouncing back and complete the first rocking cycle at around 1.7 s. The individual course traces also show that a great portion of energy is dissipated at the transition between half-cycles, i.e. when the blocks from adjacent courses impact on each other. The peak horizontal displacement of the top course is recorded at around 1.15 s and is equal to 276.4 mm whereas for the second cycle it becomes 36.5 mm at around 1.85 s, equivalent to an 87% reduction after one complete rocking cycle. The relative rocking of the upper courses with respect to the lower ones is also shown in the graphs of Fig. 17. The motion begins with the uplift of the lower course on the offshore side (Fig. 17a) and upper courses on the leeward side (Fig. 17b), until around 1.0 s. Afterwards, between around 1.0 s and 1.5 s, the only courses affected by uplift are the ones on the

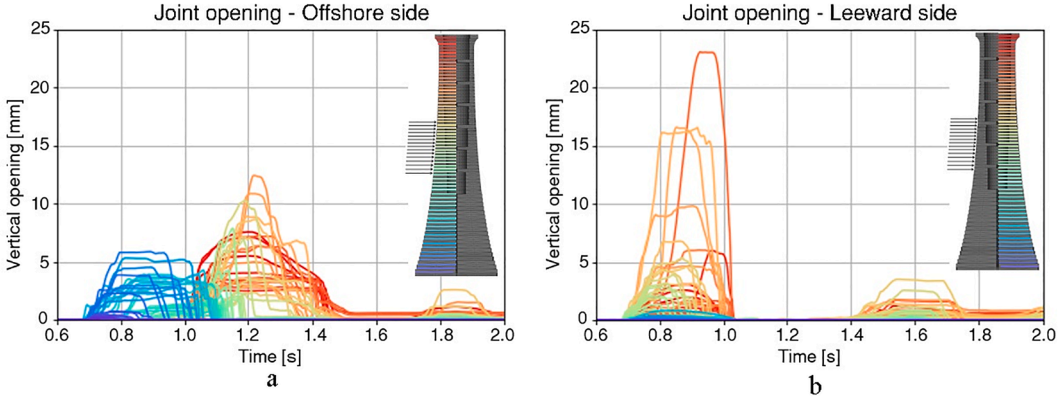

Fig. 17. Individual courses uplift for the 250YR impact: (a) offshore side; (b) leeward side.

upper portion on the offshore (Fig. 17a), hence highlighting the lag in the first half-cycle rocking motion of the upper portion in respect to the lower portion. To note that in this period there is no uplifit on the leeward side at any height.

5. Conclusions

The influence of the variability of wave impact force time-history characteristics to the structural response of Wolf Rock lighthouse is presented with the use of analytic formulations, limit state analysis and by carrying out multiple DEM analyses with wave impacts profiles generated on the basis of flume laboratory tests.

Although there is no clear transition boundary between perfectly static and dynamic condition, the uplift threshold calculated with the limit analysis method is useful for indicating the order of magnitude of wave force which is required for causing intense rocking of the lighthouse. For a plunging wave impacting the lighthouse with a force resultant at 17.99 m from its base, as the impact calculated for the 250-year return period wave, the uplift threshold is equal to 5734 kN. An important structural characteristic that contributed to the longevity of this lighthouse typology is the vertical keying, without which, it is shown that Wolf Rock would suffer sliding failure for waves of impact force around 3952 kN, a value lower than the force required to cause partial uplift and rocking. For impacts at lower heights, the difference between uplift and sliding limit is even greater.

The complex rocking motion of the lighthouse, with joints opening in different instances and internal forces developing between the blocks, makes its accurate prediction with analytic formulations very difficult. Moreover, the DEM analyses also show that in such a multi-block structure of interlocked masonry, an important amount of energy is dissipated during the rocking impacts. This is attributed to the local impact effects between courses and the friction at the multiple contact interfaces.

Regarding the wave force time-history shape, it is shown that the impact duration is of primary importance. For impacts of the same impulse, short duration waves produce lower overall displacements than longer impacts. However, it is found that the level of overall displacements and the joint opening are not correlated. The former is strongly influenced by the impact duration whereas the latter mainly depends on the maximum impact force and whether this is reached with a gradual increase or suddenly. The biggest uplift of the upper joints on the opposite of the impact side is caused by impacts which start with a sudden peak of forces, with the strongest impacts causing the greatest openings. On the contrary, impacts with gradually increasing forces cause rocking motions that resemble a rotation about only one hinge and only minor opening of the upper joints. This is clearly demonstrated by the structural response to the PARAB1 and PARAB2 impacts which have the same impulse and identical but mirrored parabolic force time-history. PARAB2, which begins with the peak force, produces an opening on the upper joints opposite of impact equal to 4.3 mm and maximum horizontal displacement on the top of 561.1 mm during the first half-cycle of rocking, whereas PARAB1 yields 0.6 mm and 429.1 mm respectively.

The theoretical 250YR impact, calculated for the 250-year return period wave on Wolf Rock, has the shortest duration of only 0.07 s but also the highest peak impact force of 51,149 kN. Compared to the other impacts of longer duration and smaller peak force, the theoretical 250YR yields the lowest levels of horizontal displacement on the top of the structure, equal to 276.4 mm. However, the theoretical 250YR also gives the highest opening, of 22.3 mm, at the upper joints opposite to the impact side. This is smaller than the height of the vertical interlocking keys and therefore the lighthouse in not in imminent risk of sliding failure.

CRediT authorship contribution statement

Athanasios Pappas: Writing - original draft, Methodology, Investigation, Software, Validation, Visualization. **Dina D'Ayala:** Conceptualization, Methodology, Writing - review & editing, Funding acquisition. **Darshana T. Dassanayake:** . **Alessandro Antonini:** . **Alison Raby:** Funding acquisition.

Declaration of Competing Interest

The authors declare that they have no known competing financial interests or personal relationships that could have appeared to influence the work reported in this paper.

Acknowledgments

The authors would like to thank the UK Engineering and Physical Sciences Research Council (EPSRC) for the financial support of the STORMLAMP project [EP/N022947/1, EP/N023285/1] and the UK & Irish General Lighthouse Authorities, in particular Trinity House, for the provision of detailed drawings and for physical access to the Wolf Rock lighthouse.

Appendix A. Supplementary material

Supplementary data to this article can be found online at https://doi.org/10.1016/j.engstruct.2020.111534.

References

[1] Smeaton J. A narrative of the building and a description of the construction of the Edystone Lighthouse with stone. London: Printed for the author by H. Hughs, sold by G. Nicol; 1791.
[2] Douglass JN. The Wolf Rock Lighthouse. (includes plates). Inst. Civ. Eng., vol. 30, 1870, p. 1–16. https://doi.org/10.1680/imotp.1870.23010.
[3] Douglass WT, Webb S, Owen GW, Redman JB, Beazeley M, Harcourt LFV, et al. Discussion on the new Eddystone Lighthouse. Minutes Proc Inst Civ Eng 1884;75:37–56. https://doi.org/10.1680/imotp.1884.21614.
[4] Goda YH, Haranaka S, Kitahata M. Study on impulsive breaking wave forces on piles. Rep Port Harb Tech Res Inst 1966;6:1–30.
[5] Watanabe A, Horikawa K. Breaking wave forces on a large diameter cell. 14th Int. Conf. Coast. Eng., Copenhagen; 1974.
[6] Sawaragi T, Nochino M. Impact forces of nearly breaking waves on a vertical circular cylinder. Coast Eng 1984:27.
[7] Tanimoto K, Takahashi S, Kaneko T, Shiota K. Impulsive Breaking Wave Forces on an Inclined Pile Exerted by Random Waves. 20th Conf Coast Eng Taipei, Taiwan 1986;20:2288–302. https://doi.org/10.9753/icce.v20.
[8] Tanimoto K, Takahachi S, Kaneko T, Shiota K. Irregular breaking wave forces on an inclined pile. Int Conf Coast Eng Conf 1986.
[9] Apelt CJ, Piorewiez J. Laboratory studies of breaking wave forces acting on vertical cylinders in shallow water. Coast Eng 1987;1:241–62.
[10] Wienke J, Oumeraci H. Breaking wave impact force on a vertical and inclined slender pile - Theoretical and large-scale model investigations. Coast Eng 2005;52:435–62. https://doi.org/10.1016/j.coastaleng.2004.12.008.
[11] Irschik K, Sparboom U, Oumeraci H. Breaking wave loads on a slender pile in shallow water. 29th Int. Conf. Coast. Eng.; 2004.
[12] Andersen T, Frigaard P. Horns Rev II, 2-D Model Tests: Wave Run-Up on Pile. DCE Contract Report No. 3; 2006.
[13] Andersen TL, Frigaard P, Damsgaard M, De Vos L. Wave run-up on slender piles in design conditionsmodel tests and design rules for offshore wind. Coast Eng 2011;58:281–9.
[14] Hall MA. Laboratory study of breaking wave forces on piles. Beach Eros Board Tech Memo 1958:106.
[15] Goda Y. Wave forces on circular cylinders erected upon reefs. Coast Eng 1973:6.
[16] Kyte A, Tørum A. Wave forces on vertical cylinders upon shoals. Coast Eng 1996;27:263–86.
[17] Hanssen AG, Tørum A. Breaking wave forces on tripod concrete structure on shoal. J Waterw 1999;125:304–10.
[18] SPM. Shore protection manual; 1984.
[19] Tu Y, Cheng Z, Muskulus M. A global slamming force model for offshore wind jacket structures. Mar Struct 2018;60.
[20] Campbell I, Weynberg P. Measurement of parameters affecting slamming; 1980.
[21] Cointe R, Armand J. Hydrodynamic impact analysis of a cylinder. J Offshore Mech Arct Eng 1987;109:237–43.
[22] Trinh Q, Raby A, Banfi D, Corrado M, Chiaia B, Rafiq Y, et al. Modelling the Eddystone Lighthouse response to wave loading. Eng Struct 2016;125:566–78. https://doi.org/10.1016/j.engstruct.2016.06.027.

[23] Banfi D, Raby A, Simmonds D, Rafiq Y, G. B. Wave impacts on the Eddystone lighthouse: a field and laboratory investigation. ICE Coasts, Mar. Struct. Break. Conf., Liverpool; 2017.
[24] Banfi D. A field and laboratory study on the dynamic response of the Eddystone lighthouse to wave loading. Ph.D. dissertation. Plymouth: University; 2018.
[25] Dassanayake DT, Raby A, Antonini A. Physical Modelling of the Effect of Shoal Geometry on Wave Loading and Runup on a Cylinder. ASCE Coast. Struct. Conf., Hannover; 2019.
[26] Douglass WT. The Bishop Rock Lighthouses. Minutes Proc Inst Civ Eng 1892;108: 207–20. https://doi.org/10.1680/imotp.1892.20193.
[27] Housner G. The behavior of inverted pendulum structures during earthquakes. Bull Seismol Soc Am 1963;53:403–17.
[28] Yim C, Chopra A, Penzien J. Rocking response of rigid blocks to earthquakes. Earthq Eng Struct Dyn 1980;8:565–87.
[29] Ishiyama Y. Motions of rigid bodies and criteria for overturning by earthquake excitations. Bull New Zeal Soc Earthq Eng 1984;17:24–37.
[30] Spanos P, Koh A. Rocking of rigid blocks due to harmonic shaking. J Eng Mech 1984;110:1627–42.
[31] D'Ayala D, Shi Y. Modeling masonry historic buildings by multi-body dynamics. Int J Arch Heritage 2011;5(4–5):483–512. https://doi.org/10.1080/15583058.2011.557138.
[32] Cundall P. A computer model for simulating progressive large-scale movements in blocky rock system. Proc Symp Int Soc Rock Mech 1971;1:132–50.
[33] Lemos JV. Discrete element modeling of masonry structures. Int J Archit Herit 2007;1:190–213. https://doi.org/10.1080/15583050601176868.
[34] Cundall P. Explicit finite difference methods in geomechanics. Proc. 2nd Int. Conf. Numer. Methods Geomech., Blacksburg, Virginia; 1976. p. 132–50.
[35] Raby AC, Antonini A, Pappas A, Dassanayake DT, Brownjohn JMW, D'Ayala D. Wolf Rock lighthouse: past developments and future survivability under wave loading Subject Areas. Philos Trans A 2019;377.
[36] Trinity House. Wolf Rock construction drawings, n.3351; 1869.
[37] Antonini A, Raby A, Brownjohn J, Pappas A, D'Ayala D. Survivability assessment of Fastnet lighthouse. Coast Eng 2019. https://doi.org/10.1016/j.coastaleng.2019.03.007.
[38] Gilleland E, Katz R. ExtRemes 2.0: an extreme value analysis package. J Stat Softw 2016;72:1–39.
[39] U.S. Army Coastal Engineering Research Center. Shore protection manual; 1977.
[40] Schweizer J, Antonini A, Govoni L, Gottardi G, Archetti R, Supino E, et al. Investigating the potential and feasibility of an offshore wind farm in the Northern Adriatic Sea. Appl Energy 2016;177:449–63.
[41] Antonini A, Archetti R, Lamberti A. Wave simulation for the design of an innovative quay-wall: the case of Vlora's harbour. Nat Hazards Earth Syst Sci Discuss 2017;17:127–42. https://doi.org/10.5194/nhess-2016-168.
[42] Goda Y. Random seas and design of maritime structures. 2nd ed. Singapore: World Scientific; 2000.
[43] Battjes J, Groenendijk H. Wave height distributions on shallow foreshores. Coast Eng 2000:40.
[44] Hansen JB. Periodic waves in the surf zone: Analysis of experimental data. Coast Eng 2005:14.
[45] Itasca Inc. 3DEC 5.0: 3-Dimensional Distinct Element Code, Theory and Background; 2013.
[46] Brownjohn JMW, Raby A, Au S-K, Zhu Z, Wang X, Antonini A, et al. Bayesian operational modal analysis of offshore rock lighthouses: Close modes, alignment, symmetry and uncertainty. Mech Syst Signal Process 2019;133:106306. https://doi.org/10.1016/j.ymssp.2019.106306.
[47] Brownjohn JMW, Raby A, Bassitt J, Antonini A, Hudson E, Dobson P. Experimental modal analysis of British rock lighthouses. Mar Struct 2018;62:1–22. https://doi.org/10.1016/j.marstruc.2018.07.001.
[48] Psycharis I, Papastamatiou DY, Alexandris A. Parametric investigation of the stability of classical columns under harmonic and earthquake excitations. Earthq Eng Struct Dyn 2000;29:1093–109.
[49] Sarhosis V, Baraldi D, Lemos JV, Milani G. Dynamic behaviour of ancient freestanding multi-drum and monolithic columns subjected to horizontal and vertical excitations. Soil Dyn Earthq Eng 2019;120:39–57. https://doi.org/10.1016/j.soildyn.2019.01.024.
[50] Psycharis I, Lemos JV, Papastamatiou DY, Zambas C, Papantonopoulos C. Numerical study of the seismic behaviour of a part of the Parthenon Pronaos. Earthq Eng Struct Dyn 2003;32:2063–84. https://doi.org/10.1002/eqe.315.
[51] Dimitri R, De Lorenzis L, Zavarise G. Numerical study on the dynamic behavior of masonry columns and arches on buttresses with the discrete element method. Eng Struct 2011;33:3172–88.
[52] Lajtai EZ, Gadi AM. Friction on a granite to granite interface. Rock Mech Rock Eng 1989;22:25–49. https://doi.org/10.1007/BF01274118.
[53] Pappas A, D'Ayala D, Antonini A, Brownjohn J, Raby A. Numerical modelling of Fastnet lighthouse based on experimental dynamic identification. Int. Conf. Adv. Constr. Mater. Syst. ICACMS-2017, Chennai; 2017.
[54] Whittaker CN, Raby AC, Fitzgerald CJ, H TP. The average shape of large waves in the coastal zone. Coast Eng 2016;14:253–64.
[55] Pappas A, D'Ayala D, Antonini A, Raby A. Rock mounted iconic lighthouses under extreme wave impacts: Limit Analysis and Discrete Element Method. 9th Int. Conf. Comput. Methods - ICCM2018, Rome; 2018.